Real World and Tropical Cyclone World. Part II: Sensitivity of Tropical Cyclone Formation to Uniform and Meridionally Varying Sea Surface Temperatures under Aquaplanet Conditions

K. J. E. WALSH,[a] S. SHARMILA,[a,b] M. THATCHER,[c] S. WALES,[a,d] S. UTEMBE,[a,e] AND A. VAUGHAN[a,f,g]

[a] *School of Earth Sciences, University of Melbourne, Melbourne, Australia*
[b] *Centre for Applied Climate Sciences, University of Southern Queensland, Toowoomba, Queensland, Australia*
[c] *CSIRO Oceans and Atmosphere, Aspendale, Australia*
[d] *ARC Centre of Excellence for Climate Extremes, University of New South Wales, Sydney, Australia*
[e] *Environmental Protection Authority Victoria, Melbourne, Australia*
[f] *ARC Centre of Excellence for Climate System Science, University of New South Wales, Sydney, Australia*
[g] *Department of Earth Sciences, University of Cambridge, Cambridge, United Kingdom*

(Manuscript received 30 January 2019, in final form 18 November 2019)

ABSTRACT

This study aims to investigate the response of simulated tropical cyclone formation to specific climate conditions, using an idealized aquaplanet framework of an ~40-km-horizontal-resolution atmospheric general circulation model. Two sets of idealized model experiments have been performed, one with a set of uniformly distributed constant global sea surface temperatures (SSTs) and another in which varying meridional SST gradients are imposed. The results show that the strongest relationship between climate and tropical cyclone formation is with vertical static stability: increased static stability is strongly associated with decreased tropical cyclone formation. Vertical wind shear and midtropospheric vertical velocity also appear to be related to tropical cyclone formation, although below a threshold value of wind shear there appears to be little relationship. The relationship of tropical cyclone formation with maximum potential intensity and mean sea surface temperature is weak and not monotonic. These simulations strongly suggest that vertical static stability should be part of any climate theory of tropical cyclone formation.

1. Introduction

There have recently been a number of advances in our understanding of the relationship between climate and tropical cyclone formation. Quantitative relationships between variations in climate variables have previously been established using statistical techniques, through the use of ''genesis potential indices'' (GPIs; Gray 1975; Menkes et al. 2012; Camargo 2013; Camargo et al. 2014). While these relationships have clearly shown some skill in representing the variations in tropical cyclone formation due to year-to-year climate variations, the different indices contain different climate variables in them. In addition, it is not clear that there is a strong relationship between changes in the GPI values and simulated changes in tropical cyclone formation as simulated by climate models in either anthropogenic climate change experiments or more idealized climate experiments (Menkes et al. 2012; Camargo et al. 2014).

Another approach to relate climate to tropical cyclone formation is through the use of fine-resolution climate model experiments; the reader is referred to Part I of this study for a review of this topic (Sharmila et al. 2020, hereinafter Part I). In Part I, the performance of one such model in simulating tropical cyclone formation was evaluated and found to have a good representation of both current climate variables and tropical cyclone formation rates. Thus, this model could be used as a tool to investigate the changes in tropical cyclone formation rates that might occur if very different climate conditions were specified. In this way, some of the numerous confounding factors in the relationship between tropical cyclone formation rates and climate variables could be removed by specifying much simpler climate conditions than exist on Earth in the current climate. In particular, we are interested in ''tropical cyclone world'' simulations, where factors that inhibit tropical cyclone

Corresponding author: Kevin Walsh, kevin.walsh@unimelb.edu.au

DOI: 10.1175/JCLI-D-19-0079.1

formation are removed wherever possible, a term that was first used in the *f*-plane simulations of Khairoutdinov and Emanuel (2013). Subsequently, tropical cyclone world simulations have been extended to β-plane and spherical geometry models [see Merlis and Held (2019) for a recent review]. These simulations have the important characteristic that they permit poleward propagation of tropical cyclones through β drift (Holland 1983). More fundamental relationships between climate and tropical cyclones therefore have the potential to be elucidated using this approach.

The idealized simulations shown here use the aquaplanet method (Hayashi and Sumi 1986), whereby all orography is replaced by ocean. This approach has been employed recently in various studies that have examined the influence of the resulting climate on tropical cyclone (TC) formation, and a recent review is contained in Merlis and Held (2019). Merlis et al. (2013) used a general circulation model (GCM) with a horizontal resolution of 50 km, combined with a slab ocean and a varying specification of ocean heat flux, to manipulate the position of the intertropical convergence zone (ITCZ), finding a strong sensitivity of TC numbers to the latitude of the ITCZ. Ballinger et al. (2015) used a similar GCM with specified and slab sea surface temperatures (SSTs) to examine the links between the position of the ITCZ and TC formation, finding that formation was increased with increased distance away from the equator of the region of maximum SST. Merlis et al. (2016) used a fine-resolution GCM to show that TC formation decreases with increasing SST for simulations with globally uniform SST. Viale and Merlis (2017) examined the relative impact of changes in TC formation caused by variations in SST, along with changes in solar and CO_2 forcing.

One method that has recently been employed for studying TC formation is the radiative–convective equilibrium framework, both rotating and nonrotating (e.g., Held and Zhao 2008; Shi and Bretherton 2014; Reed and Chavas 2015; Wing et al. 2016; Zhou et al. 2014, 2017). These runs represent a kind of ''tropical cyclone world'' in that the model domain typically fills up with TCs. This work has enabled insights to be made into the relationship between environmental forcing and TC formation. For instance, Rappin and Nolan (2012) used this framework to explain the mechanisms relating vertical wind shear to TC formation. The relationship between TC formation, vertical wind shear, and planetary vorticity was investigated by Zhou (2015), who found that for low values of planetary vorticity, TC formation was sensitive both to vertical wind shear and the thermodynamic state of the atmosphere. Higher values of planetary vorticity were found to enable the incipient TC vortex to resist the disruptive effects of vertical wind shear. Along these lines, Fedorov et al. (2019) recently employed a cloud-resolving idealized model to investigate the effects of varying meridional SST gradients on TC formation, with the rationale that meridional gradients of SST are related to vertical wind shear through the thermal wind relationship. They found that when the gradient is substantially reduced, the number of TCs increases, accompanied by a decrease in the vertical wind shear, a factor well known to be related to TC formation (e.g., Gray 1968, 1975).

Here, we extend these ideas to a series of GCM experiments that have a less idealized representation of the model dynamics than that specified in Fedorov et al. (2019), as that study employed a zonally periodic β plane and an imposed scaling of the vertical momentum equation. Specifically, the version of the GCM used here is identical to that used in Part I and does not use any dynamical rescaling factors. In addition, an important novel aspect of the present paper is that we quantify the relationship between climate variables and TC formation to compare the simulated relationships with those derived statistically in the current climate, as formulated in the GPIs (see the appendix) in order to inform the basic structure of a climate theory of TC formation. Note here that we do not examine issues associated with the interactions between TC intensity and SST variations, which have been well examined in previous work (e.g., Schade and Emanuel 1999; Ma et al. 2013, 2017). Examination of the simulated TC intensity distribution by the model showed that like many climate models of this resolution, the simulated storms were weak compared with observed storms (not shown). Thus we focus on the relationship between climate and TC formation.

The paper is organized as follows: section 2 describes the model and the experimental framework, as well as the TC detection method. The key results from idealized simulations are presented and discussed in section 3, and section 4 offers a list of important concluding remarks.

2. Model, data, and method

Model and experimental design

We use the atmospheric component of the Australian Community Climate and Earth-System Simulator coupled general circulation model (ACCESS) based on the Met Office Unified Model (UM v8.5) Global Atmosphere (GA6.0) (Walters et al. 2017), denoted here as ACCESS. The model includes a dynamical core with a semi-implicit semi-Lagrangian formulation, a comprehensive suite of physical parameterizations split into slow processes (radiation, large-scale precipitation, and gravity wave drag) and fast processes (atmospheric boundary layer, turbulence, convection, and land surface coupling), including the prognostic cloud fraction and prognostic condensate

TABLE 1. Names and description of each experiment.

Simulation	Description
CSST25	Constant global SST of 25°C
CSST27.5 (CTRL)	Constant global SST of 27.5°C
CSST30	Constant global SST of 30°C
VWS_DG60	Constant SST of 40°C but linear decreasing SST gradient poleward of 60° lat
VWS_SG60	As in VWS_DG60 but with a stronger SST gradient
VWS_G30	As in VWS_DG60 but SST gradient imposed poleward of 30°
VWS_G5	As in VWS_G30 but SST gradient imposed poleward of 5°
VWS_SG5	As in VWS_G5 but with a stronger SST gradient

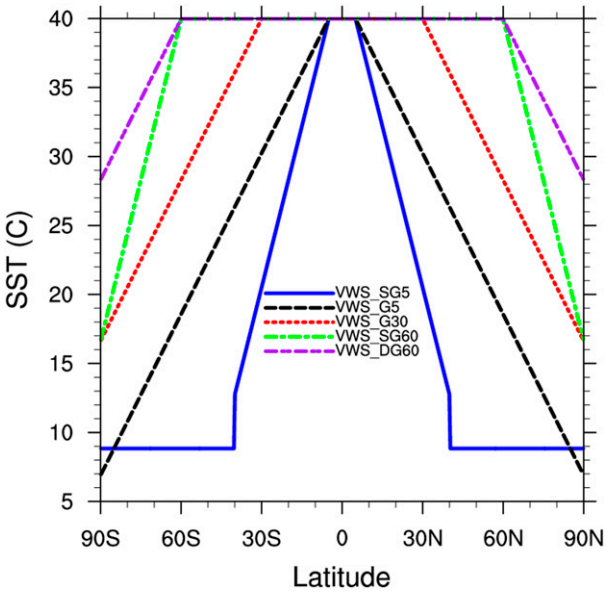

FIG. 1. Zonally averaged SST values for the various meridional "gradient SST" runs (°C). Experiment names are described in Table 1.

(PC2) scheme (Wilson et al. 2008). The model also uses the radiation scheme of Edwards and Slingo (1996), a boundary layer scheme that represents mixing over the full depth of the troposphere (Lock et al. 2000), and a community land surface model, the Joint U.K. Land Environment Simulator (JULES; Best et al. 2011). More model details can be found in Walters et al. (2017).

The experimental design involves specifying a number of different SST fields and examining the resulting effects on TC formation. A baseline study is performed with constant SST uniformly distributed over the entire globe, with three different SST values specified: 25°, 27.5°, and 30°C (Table 1). At the same time, radiative forcing, including its seasonal variation, as well as rotation, are left at Earth values. In this suite of experiments, we are primarily interested in the ratios of the number of TCs generated between the experiments rather than the absolute values, as we have already established in Part I that the model has a good simulation of TC numbers in the current climate. We also investigate the effects of various idealized meridional SST gradients as a way of specifying different wind shear values and locations, through the thermal wind relationship (Table 1 and Fig. 1). In this way, we aim to quantify the relationship of wind shear and other variables to TC formation. Vertical wind shear is calculated between the 850- and 200-hPa levels.

The method for detection of TCs in the model output is very similar to that described in Part I except that there is no latitude restriction on formation, and slightly modified criteria are imposed on the TCs. The mean wind speed in the region 700 km × 700 km square around the center of the storm at 850 hPa must be at least 3 m s^{-1} greater than at 300 hPa, as opposed to zero in Part I; and the duration requirement is increase to 48 h, from 24 h. These changes have very little effect on the number of detected TCs shown in Part I but at the same time the changes do eliminate a number of asymmetrical midlatitude disturbances that are clearly not TCs but that temporarily satisfy the detection requirements imposed in Part I.

The experiments have only been run for five years. Simulations are performed beginning at initial atmospheric conditions corresponding to SSTs of 1 September 1988, which themselves have been produced from a spinup run of 63 years starting from 1 September 1950 forced with AMIP-II SSTs (Kanamitsu et al. 2002). Subsequently, a further 4-month spinup period starting at 1 September 1988 is discarded from the analysis. The model runs are then analyzed for a total of five model years. The rationale for analyzing such short model runs for these experiments as compared with those required to generate a climatology (typically at least 30 years) is that the changes in the surface forcing are so large that the response of the model to the forcing should be apparent after only a small spinup period. To show this, we examine whether the year-to-year variability is larger than the response to the imposed perturbation by comparing the year-to-year variation of vertical wind shear in the constant SST runs (Table 2). The vertical wind shear is here defined as the magnitude of the vector difference of winds between 850 and 200 hPa. Table 2 shows that the standard deviation of the interannual variability of wind shear in the constant SST runs is considerably less than the difference in wind shear between the runs, with the model response being larger by at least a factor of 3. Thus, we believe that the model response in these relatively short runs is robust and not an artifact of year-to-year variability.

TABLE 2. Comparison of the interannual variability of the zonal annual average of vertical wind shear at latitude 26.25° with the model response.

	25°C	27.5°C	30°C	25°–27.5°C	30°–27.5°C
1989	8.44	7.82	6.54	0.63	−1.28
1990	8.45	7.56	6.33	0.89	−1.22
1991	8.92	8.11	6.51	0.80	−1.61
1992	8.34	8.26	6.48	0.09	−1.78
1993	8.94	7.75	6.21	1.19	−1.54
Mean	8.61	7.90	6.41		
Std dev	0.25	0.25	0.12		

3. Results and discussions

a. Results from constant global SST experiments

Figure 2 shows a comparison between the area-weighted simulated TC genesis (TCG) of simulations with constant tropical SST over the entire globe, for different values of SST. There is a clear decrease of the TC formation rates as the surface temperature increases. The geographical pattern of TC formation is also different from that seen in the ''real-world'' terrestrial current climate (Part I). In the so-called real-world simulation, TCs form within the latitude band of 5°–30°, as TC formation is inhibited near the equator because of very low Coriolis force (e.g., Gray 1968, 1975). However, in these constant global SST experiments in the aquaplanet configuration, TC formation is reduced within 25° of the equator, and the maximum formation rate occurs in the midlatitudes, generally poleward of 40° latitude. Fundamentally, in these constant SST experiments, this is due to the lack of baroclinicity in the midlatitudes and the resulting lack of vertical wind shear. As demonstrated in the area-weighted latitudinal distribution of zonally averaged TCG density (Fig. 3a), there is also a gradual but systematic decrease in the number of midlatitude and polar TCs with an increase in specified global SSTs, as well as in the tropical regions. Table 3 shows the number of TCs (as annual means) in various latitudinal bins for simulations under fixed global SST conditions. Using the run with SST fixed at 27.5°C as our control experiment (denoted CTRL, since it is the middle SST run of the three constant SST runs), we see that for this control simulation annually the total number of TCs is around 1800, which is 22 times the observed global annual rate of about 80 TCs. We naturally expect to see more TCs under globally uniform tropical SSTs than in the terrestrial climate, since factors that lead to the reduction in TCs in the current terrestrial climate, such as the presence of land and considerably larger wind shear due to meridional SST gradients, are eliminated or reduced in these constant SST runs.

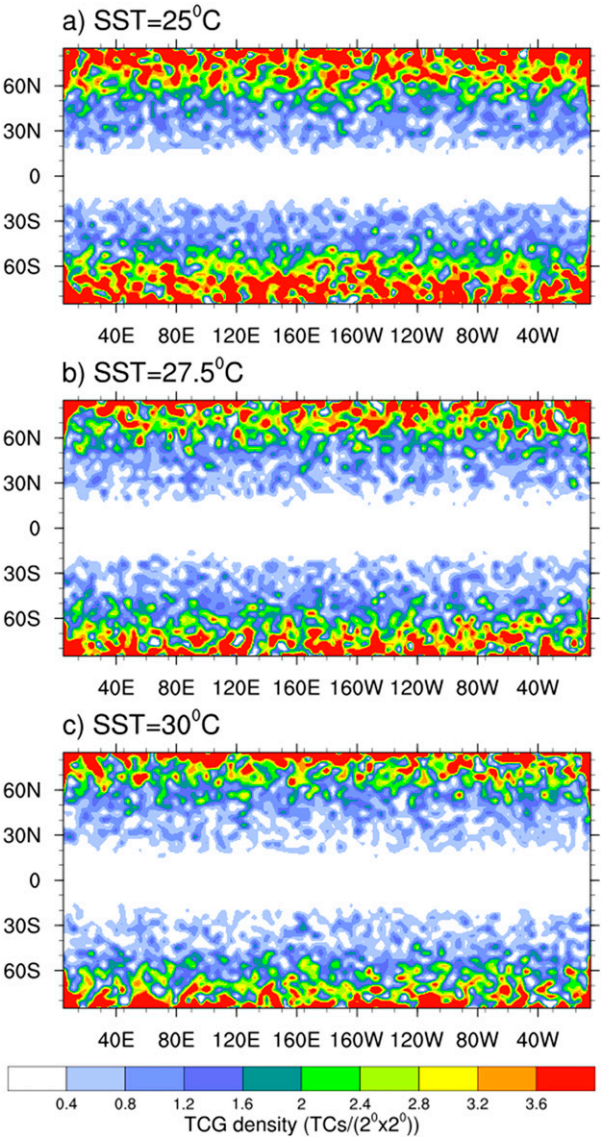

FIG. 2. The TC genesis density per 2° × 2° box (area weighted) per 5 years for all three globally uniform SST scenarios.

Comparing the three globally uniform SST runs, we note in Table 3 that reducing the SST from 27.5° to 25°C results in a 26% increase in number of simulated TCs (up to 2277 TCs) whereas increasing the SST to 30°C results in a 13% decrease in simulated TCs (down to 1586 TCs). Since land is absent in these runs and because of the constant global SSTs imposed, we expect to see approximately the same number of TCs simulated in each hemisphere, as seen in Table 3. In each hemisphere, a significant portion (at least 88%) of the TCs are formed poleward of 30° latitude, with only about 10% of the TCs being formed equatorward of 30° latitude. Interestingly, the total number of TCs forming equatorward of 30°S is

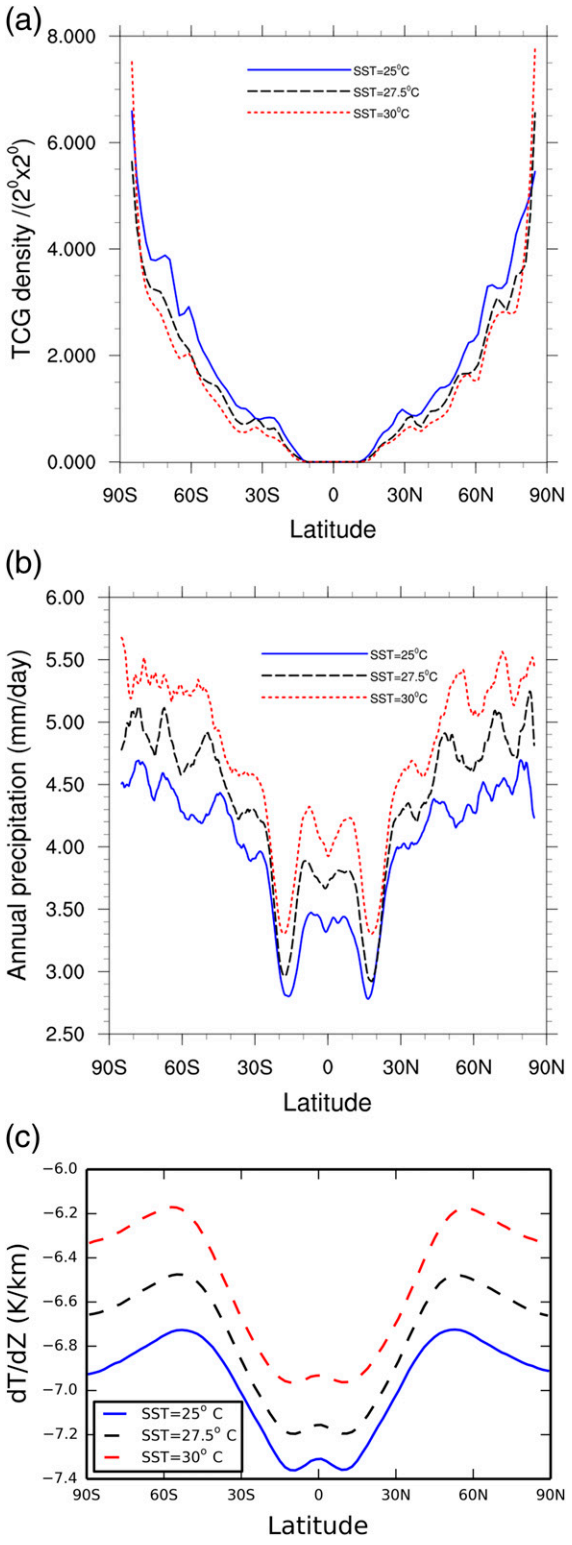

FIG. 3. Globally uniform SST scenarios for (a) zonally averaged latitudinal distribution of TCG density (number of TCs per 5 years per 2° × 2° grid box; area weighted), (b) zonally averaged zonal mean distribution of annual mean precipitation (mm day^{-1}), and (c) zonally averaged latitudinal distribution of annual mean lapse rate (°K2009;km^{-1}) between 850 and 200 hPa. Note that omega greater than zero indicates subsidence.

TABLE 3. Number of TCs simulated per year under various constant global SST scenarios for each latitudinal bin where G = global, SH = Southern Hemisphere, NH = Northern Hemisphere, SH1 = 0°–30°S, SH2 = 30.01°–60°S, SH3 = 60.01°–90°S, NH1 = 0°–30°N, NH2 = 30.01°–60°N, and NH3 = 60.01°–90°N.

Expt	G	SH	NH	SH1	SH2	SH3	NH1	NH2	NH3
25°C	2277	1152	1125	148	514	489	148	507	469
27.5°C	1808	909	899	104	410	394	94	409	395
30°C	1586	784	802	82	345	356	81	354	366

much closer to the observed terrestrial formation rate in those latitudes, being only somewhat greater than the terrestrial rate. This suggests that the terrestrial formation rate over the tropics proceeds at a similar rate to that seen in the aquaplanet runs, but that TC formation in the terrestrial climate in the tropics is limited by land regions and outside of the tropics by hostile atmospheric conditions.

To help to explain this result, we note that the global pattern of precipitation for each run (Fig. 3b) shows an increase with increasing SST, as expected due to the inevitable increase in global evaporation with increased SST. Greater precipitation will lead to greater latent heat release in the mid to upper troposphere due to increased condensation there, thereby warming the upper troposphere more than the lower troposphere and leading to the potential for a decrease in the atmospheric lapse rate. Examining the lapse rate changes between the three runs (Fig. 3c) indicates this clear decrease of lapse rate with increasing SST. It has been previously hypothesized (Sugi et al. 2002) that a decrease in lapse rate associated with a warmer surface will likely lead to a slowdown in the vertical circulation of the tropics, leading to a suppression of TC formation. The fundamental reason is that the increase in precipitation caused by increased SST is not as large as the increase in atmospheric moisture, and this is consistent with a decrease in the vertical circulation of the atmosphere (Knutson and Manabe 1995). The decrease in lapse rate is driven by increased latent heat release in the upper troposphere associated with increased precipitation. A measure of vertical circulation is the vertical pressure velocity at 500 hPa, here represented by omega (Fig. 4). For the three constant SST runs, there are minor differences between omega between them (Fig. 4b) but they all have similar mean patterns (Fig. 4a). This shows maximum descent (positive omega) in tropical and subtropical regions, with mostly ascent (negative omega) elsewhere. There is a relationship between omega and TCG (see also Fig. 8b, below), with more upward vertical velocity leading to more TCG. A competing theory (Emanuel 2013) suggests that a decrease in TCG is related to an increase in saturation deficit (and Fig. 9b, below, is

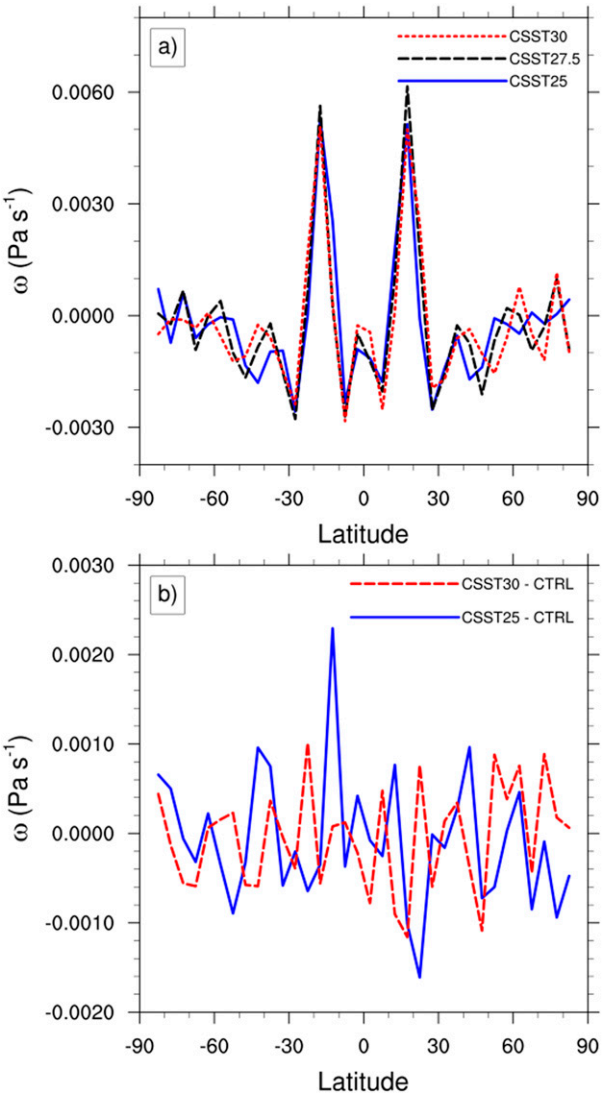

FIG. 4. Zonal mean distribution of (a) annual mean omega (Pa s^{-1}) at 500 hPa for globally uniform SST runs; (b) as in (a) but the difference between runs, SST = 30°C minus SST = 27.5°C run (red line), where the CSST27.5 simulation is denoted the control or CTRL simulation here, and SST = 25°C minus SST = 27.5°C (blue line), in 5° latitude band averages. Note that omega greater than zero indicates subsidence.

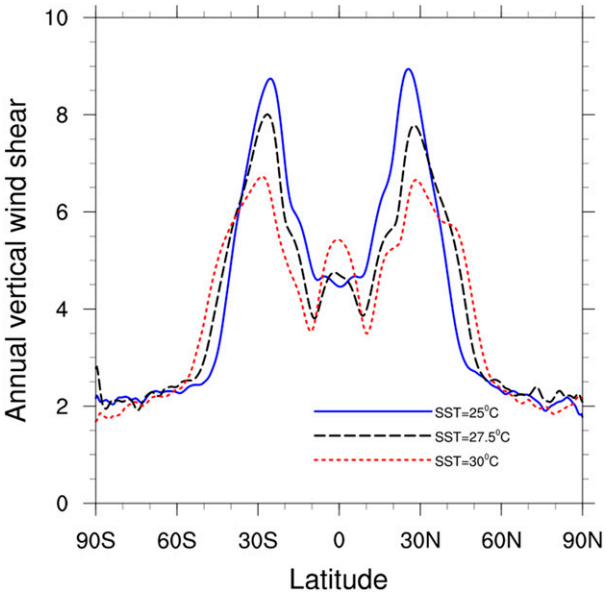

FIG. 5. Zonally averaged latitudinal distribution of annual mean vertical wind shear (m s^{-1}) for globally uniform SST runs.

certainly consistent with this theory), although note that Emanuel (2013) defines saturation deficit in terms of moist static energy deficit rather than relative humidity deficit.

Another climate variable that is well known to be related to rates of TC formation is vertical wind shear. Nevertheless, analysis shows that this variable is not a strong factor in explaining the changes in formation rate between the constant SST runs, as wind shear mostly decreases as SST increases (Fig. 5), particularly in the subtropics. Vertical wind shear can increase due to a meridional temperature gradient through the thermal wind relationship, but that is not relevant here at the surface because constant SST is specified in these runs. However, because we retain Earth-like insolation, which has a meridional gradient, and because differences in surface temperatures will give different rates of latent heat release in the upper troposphere, there is a meridional temperature gradient aloft (not shown), and this is what is causing the increase in wind shear as surface temperature decreases in these simulations.

b. *Results from meridional gradient SST experiments*

Here, we impose various meridional gradients of SST onto the aquaplanet surface to examine the effects of the model-generated vertical wind shear on the simulated TC formation rates. The main purpose of these experiments is to quantify the relationship between TC formation and vertical wind shear, at various mean SST values. Figure 6a again shows the various meridional SST gradients imposed in the different experiments (see Fig. 1) for easy comparison to the other panels in this figure. Figure 6 also shows the relationship between the SST gradients and TC genesis, shear, and precipitation. As expected, the strength of the meridional SST gradient appears closely related to the shear (Fig. 6c), with largest values of shear for runs VWS_SG5 and VWS_G5, which have the largest region of strong SST gradients. Climatological shear in the subtropical regions of VWS_G5 can exceed 60 m s^{-1}, which is considerably larger than the largest climatological shears simulated in the terrestrial climate runs using this model (Part I). In contrast, shear for runs VWS_DG60 and VWS_SG60 is modest, not exceeding 10 m s^{-1}. The accompanying

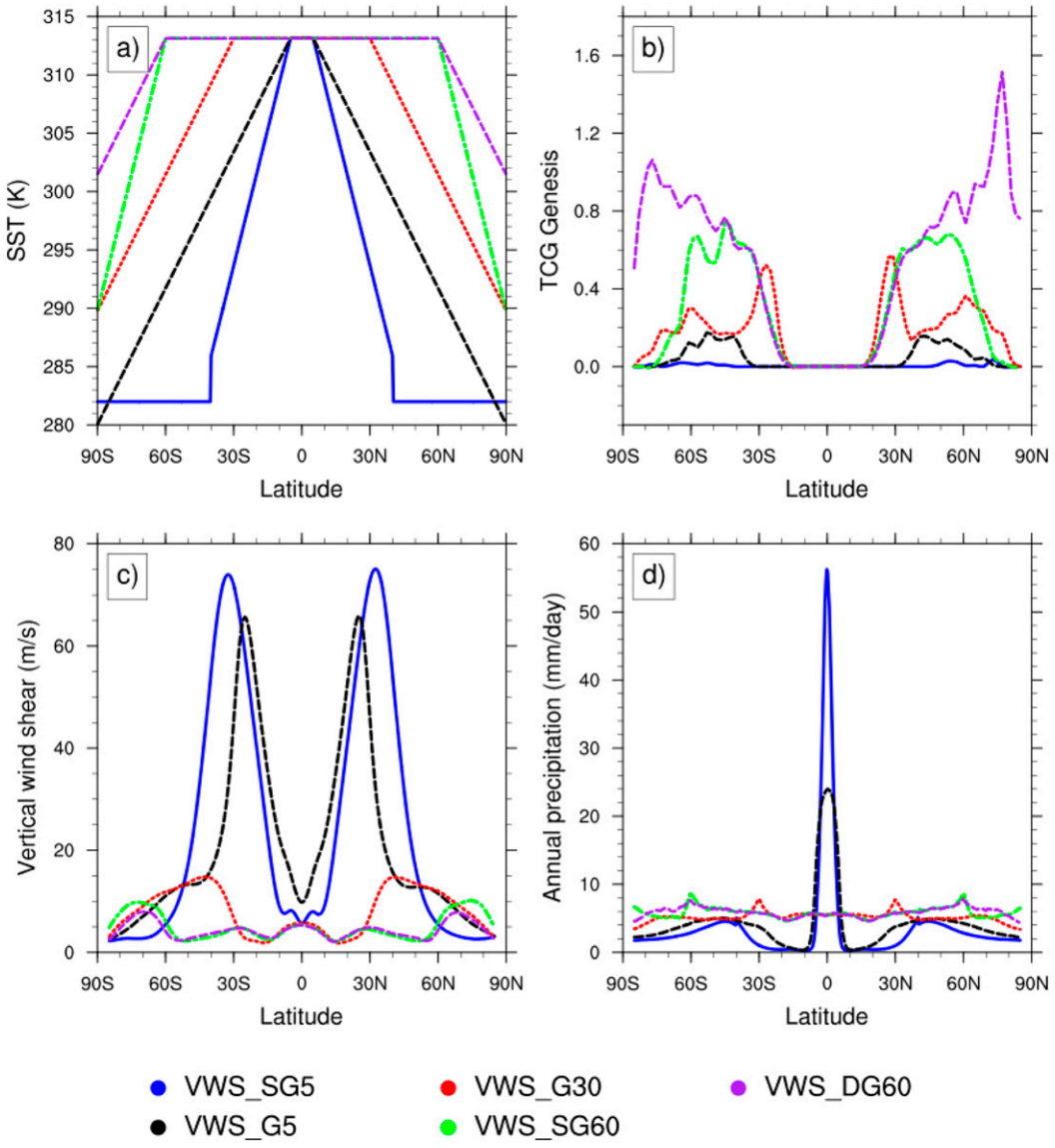

FIG. 6. Zonal mean (a) SSTs for various meridional SST gradient simulations, (b) TC genesis density (number of TCs per 3 years per 2° × 2° box, area-weighted), (c) vertical wind shear (m s^{-1}), and (d) precipitation (mm day^{-1}).

effects on TC genesis (Fig. 6b) are dramatic: for instance, run VWS_SG5, which has the strongest SST gradients, only has substantial TC formation poleward of about 40°, where the meridional SST gradient is zero. Precipitation in the high-SST gradient runs VWS_SG517 and VWS_G5 (Fig. 6d) is highly concentrated in the equatorial region, while it is more evenly spread between the latitudes in the other runs. This concentration of low-latitude precipitation is likely due to the strong SST gradient near the equator in these runs, as Fedorov et al. (2019) showed that the precipitation maximum in their simulations occurred at the apex of the specified SST gradient and that the size of the precipitation peak increased with increased gradient, which is also seen here, with run VWS_SG5 having a larger peak than run VWS_G5.

c. *Global average results*

So far, we have examined the latitudinal variation of TC genesis compared with various related atmospheric variables. To gain a global overview of these relationships, we now show globally averaged plots for TC genesis and different climate variables. Figure 7 shows the quantitative global average relationships between TC genesis, vertical wind shear, precipitation, and SST, for global mean values. The relationship between TC genesis and wind shear is not linear (Fig. 7a), with TC

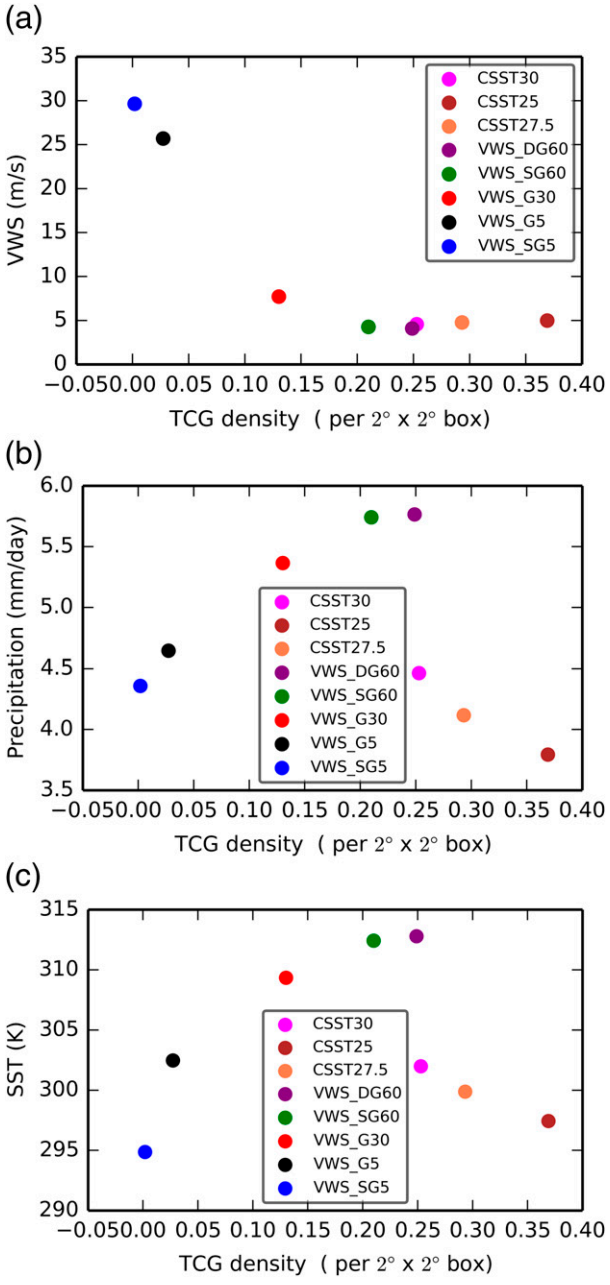

FIG. 7. Relationship between global mean TC genesis density (per 2° × 2° box per three years, area-weighted) and (a) global mean vertical wind shear, (b) precipitation, and (c) global mean SST.

formation increasing nonlinearly as wind shear decreases. TC formation approaches zero as the global mean wind shear rises to 20 m s^{-1}. Also, in included in this figure are the constant SST runs (the CSST runs, all of which predictably have low but not zero shear). Shear appears to have no relationship to TCG variations for global mean shear values less than a "shear threshold" of about 5 m s^{-1}, but for shear greater than this, the TCG rate falls rapidly. The relationship between TCG and

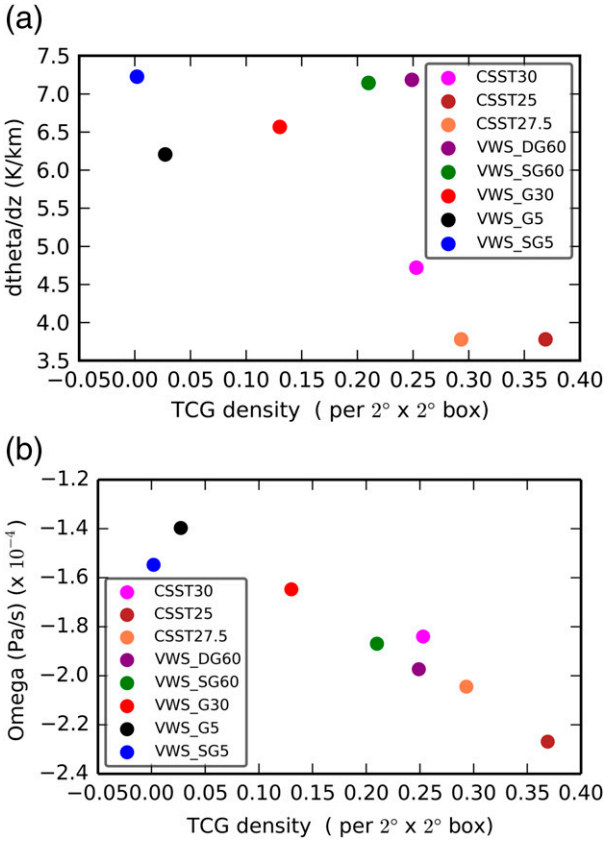

FIG. 8. As in Fig. 7, but for (a) vertical potential temperature gradient between 1000 and 200 hPa (°K2009;km^{-1}) and (b) omega at 500 hPa (Pa s^{-1}).

precipitation (Fig. 7b) is not as clear-cut and is clearly being influenced by both the pattern of the SST and its values (Fig. 7c). As the meridional SST gradient decreases, precipitation increases but in general the global mean precipitation rate follows the global mean SST, as does the latent heat flux (not shown).

Figure 8 shows the same as Fig. 7 but for vertical potential temperature gradient between 850 and 200 hPa, as a measure of atmospheric stability, as well as omega at 500 hPa. There is a clear association between increased stability and reduced TCG (Fig. 8a). Run VWS_SG5 is the most stable run and has the least TC formation, while run CSST25 (with constant SST at 25°C) is the most unstable and has the most TC formation. This relationship also holds for runs that demonstrate little relationship with vertical wind shear, as those runs are below the "shear threshold" mentioned above: comparing Fig. 8a with Fig. 7a, as stability increases between runs CSST30 and VWS_SG60, TC formation decreases, whereas a decrease in TC formation between these two runs is not accompanied by any substantial decrease in shear. This appears to indicate that below this shear

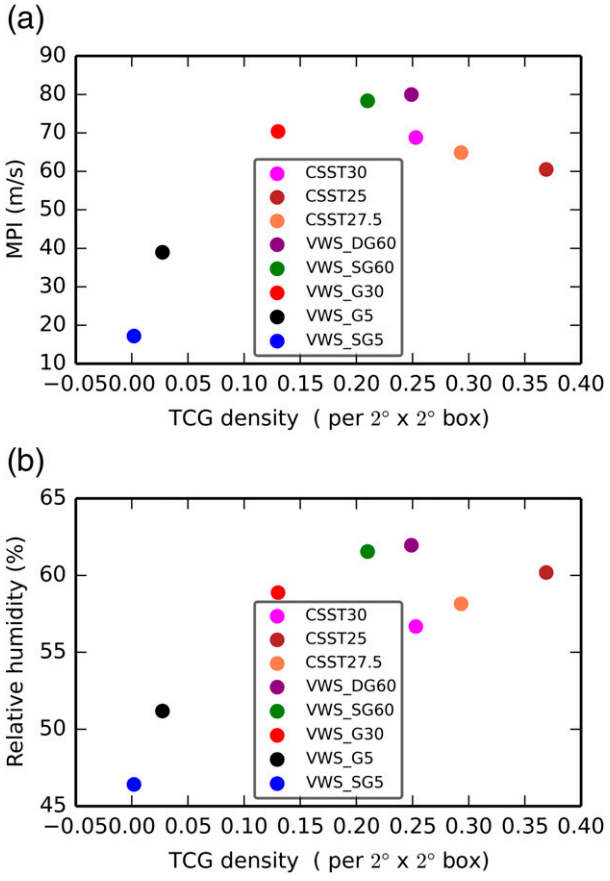

FIG. 9. As in Fig. 7, but for (a) MPI and (b) 700-hPa relative humidity.

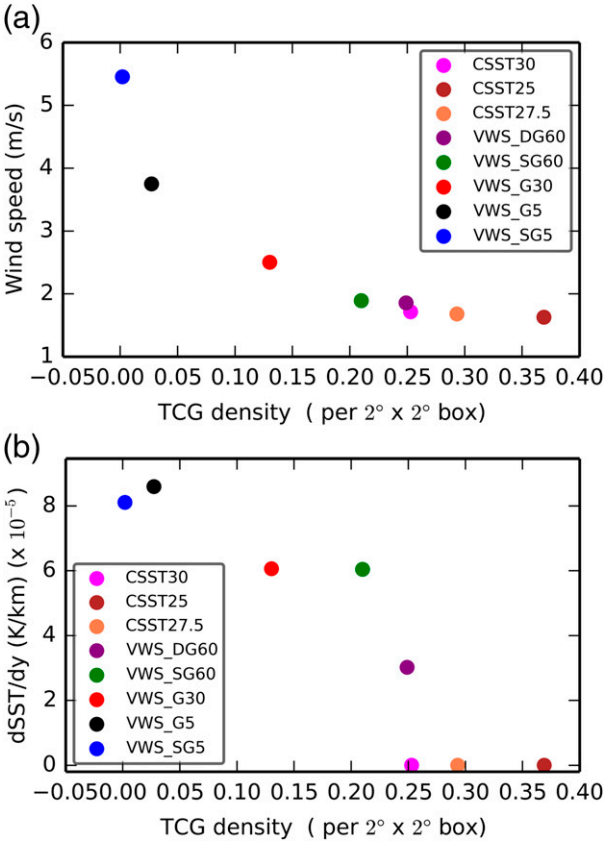

FIG. 10. As in Fig. 7, but for (a) 10-m surface wind speed and (b) mean hemispheric meridional gradient of SST.

threshold, global mean shear is not a limiting factor for TC formation. Figure 8b shows the same for omega, as this indicates more TC formation with increased mean ascent (i.e., more negative omega), although the relationship is not as strong as it is for stability, and it may be that the two are related only through other variables that are not known at present. Figure 9 shows the same for two other components of some GPIs, the maximum potential intensity (MPI; Bister and Emanuel 1998) and the 700-hPa relative humidity. The global mean MPI (Fig. 9a) appears to be dominated by the SST variation shown in Fig. 7c, although there is less decrease of MPI with increasing TCG than SST. Similarly, the relative humidity (Fig. 9b) has some relationship to TCG, with lower values generally associated with lower TCG, although like the MPI there is a relative humidity threshold above which there is no relationship with TCG.

An issue that has arisen periodically in the literature is the amount of energy extracted by TCs from the climate system, as a potential means of putting a climate-related constraint on rates of TC formation (e.g., Held and Zhao 2008; Kang and Elsner 2015). Figure 10a shows the mean 10-m surface wind speed versus TC formation rates. There is an inverse relationship between the two variables, with more TCs giving a lower average surface wind speed. This shows that the TC winds themselves are not dominating the global mean low-level wind speed, as the global mean of this variable is actually lowest for the runs with the largest number of cyclones. This result may be related to the runs with a more baroclinic environment having higher global mean low-level wind speeds but fewer tropical cyclones. A similar relationship is thus seen in Fig. 10b, which shows the global mean of the meridional gradient of SST (the main constraint in these simulations and an indicator of baroclinicity) versus TCG. Like the relationship with vertical wind shear (Fig. 7a), a larger meridional SST gradient is associated with lower TCG, and in addition for the constant SST runs, other factors such as stability changes are also causing changes in TCG rates.

We have also examined the same relationships shown in Figs. 7–10 for the region between 30°S and 30°N. The rationale for doing so is that these are the latitudes in the terrestrial climate where TCs overwhelmingly form.

The results (not shown) are very similar to the global plots in that the functional relationships between the variables are almost the same. An exception is the precipitation relationship, with more rainfall in the low-latitude region for the experiment with the steepest meridional SST gradient at low latitudes (VWS_SG5). This result is related to the amplification of the ITCZ by the increased meridional temperature gradient (e.g., Ballinger et al. 2015). The lowest rainfall amounts in this region are for the global constant SST runs.

4. Discussion and concluding remarks

In this study, a fine-resolution atmosphere-only climate model is forced by idealized representations of sea surface temperatures and the resulting relationships between climate and tropical cyclone formation are examined. There is general agreement between some of these results and those of previous similar work. Ballinger et al. (2015) found an increase in tropical cyclone formation with increasing upward vertical velocity, similar to that shown in Fig. 8b, although their results were for a selected latitude band. Other variables have a more complex relationship with tropical cyclone genesis (TCG). For the constant SST runs, there is a decrease in TCG associated with an increase in SST (Fig. 7c), as also found by Merlis et al. (2016). For these runs, the increase in SST is associated with a clear increase in vertical static stability (Fig. 3c). For runs with spatially varying SSTs, however, the relationship is the opposite: higher global mean SST is associated with higher TCG. A much stronger relationship with TCG is found with stability for all runs (Fig. 8a). In addition, Fedorov et al. (2019) found in their idealized model experiments that a strong meridional gradient of SST was associated with a strong ITCZ, and that is apparent here also in Fig. 6d. There is strong preponderance in the constant SST runs of midlatitude and polar TCs, as also found by Chavas et al. (2017) in their simulations. In our simulations, these systems are easily identifiable as TCs by their strongly symmetrical circulations (not shown), in addition to being detected by the automatic detection system used here. Note that Merlis et al. (2016) found that TCG mostly occurred in the subtropics in their simulations, although they used spatially uniform insolation whereas our insolation is meridionally varying.

The relationship between vertical velocity, lapse rate, and tropical cyclone formation has been previously investigated in the terrestrial climate. Murakami and Wang (2010) note that including a vertical velocity (omega) term in a modified version of the Emanuel and Nolan (2004) GPI yielded improved results. Kim et al. (2011) analyzed NCEP reanalyses (Kalnay et al. 1996) to show that in the western North Pacific, regions of decreased tropical cyclone formation were associated with decreased vertical velocity in the midtroposphere and negative SST anomalies. Regions with negative SST anomalies would typically be associated with decreased lapse rate, due to the relatively constant upper-troposphere temperatures in the tropics (the ''relative SST'' argument; Vecchi and Soden 2007). Thus there should be a local relationship between regions of decreased lapse rate and decreased vertical velocity (increased omega) in regions where tropical cyclones form. Nevertheless, this argument does not assist an understanding of what happens when the entire tropical surface region warms or cools, as it does in some of the sensitivity experiments above, as that violates the assumptions of the relative SST argument because the tropical upper troposphere temperature also changes due to systematic changes in tropical SSTs and the accompanying nonlinear change in upper-tropospheric latent heat release and thereby upper troposphere temperature. It has been further shown here that variations in both omega and lapse rate are related to the variations in tropical cyclone formation (Fig. 8). Nevertheless, the relationship between omega and lapse rate is not perfect and clearly other variables are influencing this relationship, although this has not been investigated here. We have investigated this further by examining this relationship for subdaily data (not shown), but the relationship is very noisy and clearly indicates a number of competing physical variables. In addition, at present we do not separate the environmental and tropical cyclone vertical circulations in the calculation of the global-average omega values, which could be a further reason for the variation in the relationship between omega and TCG. Designing GCM experiments to test the effect of fixed stability on TCG is challenging because of the strong tendency of the GCM to establish its own stability climatology. It is possible that an experiment using a relaxation back to an imposed stability profile might address this issue but we have not attempted this here.

Another limitation of this study is the inclusion of seasonally varying radiative forcing at Earth values, rather than implementing a uniform radiative forcing. This imposes an upper-tropospheric meridional temperature gradient even in the constant global SST simulations, although this gradient is rather modest compared with the imposed SST gradients in the ''gradient'' runs (not shown). It would be useful to compare these results to additional experiments in which there are no seasonal variations in radiative forcing. It would also be useful to examine the impact of the specification of a constant value of Coriolis parameter (e.g., Chavas et al. 2017), instead of the Earth-like latitudinal variation of Coriolis used here.

In principle, it seems that it would be possible to use idealized GCM experiments in an aquaplanet configuration to extract functional relationships between the various variables and tropical cyclone formation, to test the various GPIs and determine whether they are predictive of the tropical cyclone formation rate in very different climates, as well as in the terrestrial current climate for which they are derived. For instance, Fig. 7a does appear to show a nonlinear inverse relationship between shear and TCG, while the Emanuel and Nolan (2004) index similarly has an inverse square relationship, as does the Bruyère et al. (2012) index. The Tippett et al. (2011) index has shear as a negative exponential. Figure 8a shows that there is a clear nonlinear relationship between vertical static stability and TCG. The Tippett index includes a variable that might be regarded as related to stability, namely the relative SST, while the Royer et al. (1998) index explicitly includes stability as a variable. Royer and Chauvin (2009) include a convective potential term that might be regarded as a proxy for stability. Thus there is some support for a climatological relationship between mean stability and TCG. In contrast, the idealized experiments of Chavas and Emanuel (2014) did not find a relationship between stability and storm structure, although whether these results would be transferrable to an examination of global TCG is unclear at this time. A variable that we have not examined in this study is saturation entropy deficit (Emanuel 2010), although given that it increases as the midtroposphere dries, it should have the same basic relationship to TCG as for relative humidity; that is, increased deficit should be associated with decreased TCG. The exact functional form of the relationship between saturation entropy deficit and TCG is likely to differ from the relationship between relative humidity and TCG shown in Fig. 9b, however.

For MPI, the relationship with TCG is not monotonic (Fig. 9a). The Emanuel and Nolan (2004) GPI (see the appendix) has formation related to the cube of the MPI, as does the Bruyère et al. (2012) index. The Tippett index does not include MPI, but instead includes an exponential dependence on relative SST, which has also been previously shown to be a proxy for MPI (Emanuel and Sobel 2013). Relative humidity appears to have some relationship to cyclogenesis (Fig. 9b), although above a certain threshold of relative humidity there appears to be little relationship, in agreement with the results of Bruyère et al. (2012). To make a thorough comparison between the results shown here and the GPIs, though, would require comparison of the geographical patterns of climate variables and associated correlations with the geographical patterns of TCG in these runs, along the lines of how the GPIs are formulated from current terrestrial climate observations. This is beyond the scope of the current study.

The strongest relationship between global climate and global TCG is with vertical static stability. Thus, it would seem reasonable that this variable would need to be a part of any climate theory of tropical cyclone formation. There is also a consistent although slightly weaker relationship with midtropospheric vertical velocity, although this is also likely to be physically related to stability. An association with wind shear also exists, but only for global mean shear above a threshold. Relationships between TCG and MPI, and TCG and SST, are less consistent. In comparing these results with a similar analysis using observations (Sharmila and Walsh 2017; their Fig. 12), it is seen that vertical wind shear and omega also had generally more consistent relationships with TCG than MPI and SST. We did not test stability in that previous study.

In summary, a fine-resolution atmospheric climate model is used to study the impact of different specifications of SST patterns on tropical cyclone formation in an aquaplanet configuration. The main conclusions of this study are as follow:

- Tropical cyclone formation decreases with increasing SST in constant global SST aquaplanet runs. There is a clear relationship in these runs between increasing SST and increasing stability, and increased stability is also clearly related nonlinearly to decreased tropical cyclone formation when all runs are considered. Increased tropical cyclone formation is also associated with increased global mean midtropospheric upward vertical velocity, although this relationship is less strong.
- There is an inverse relationship between tropical cyclone formation and vertical wind shear, but for low values of global mean wind shear there is no clear relationship, implying that there is a lower threshold of wind shear below which it does not strongly affect tropical cyclone formation rates.
- Strong meridional SST gradients near the equator are associated with a strongly concentrated ITCZ, in agreement with previous idealized model results.
- Simulations with a very large number of tropical cyclones have lower global mean low-level wind speeds, implying that large numbers of tropical cyclones appear to be extracting energy from the mean flow.

To conclude, we find that this idealized modeling framework has significant potential to establish firmer relationships between climate variables and tropical cyclone formation and can be helpful for the development of climate theory of tropical cyclone formation. Further simulations have been performed that begin to bridge the gap between the highly idealized

aquaplanet simulations shown here and the terrestrial climate simulation discussed in Part I. Specifically, these simulations include a realistic terrestrial gradient of SST, based on a zonal average of AMIP-II data, with various representations of Earth-like topography. Results from these simulations will be discussed in future papers.

Acknowledgments. The authors acknowledge discussions with Ian Simmonds and the comments of four anonymous reviewers. The authors thank the Australian Research Council for funding this work under Discovery Project DP15012272. Author Sharmila acknowledges present support from the Northern Australia Climate Program at the University of Southern Queensland/Bureau of Meteorology, Australia. The climate model used in this study was supplied by the ACCESS modelling team, with the support of the ARC Centre of Excellence for Climate System Science. Author Vaughan acknowledges past support from the ARC Centre of Excellence for Climate System Science. The simulations and analyses were performed on the National Computational Infrastructure system, supported by the Australian Government. Figures are prepared using the free software NCL and Python. Model output from these simulations is available for analysis by contacting the corresponding author.

APPENDIX

Specification of GPIs

The Emanuel and Nolan (2004) index is defined as follows:

$$\mathrm{EN} = |10^5\eta|^{3/2}\left(\frac{H}{50}\right)^3\left(\frac{V_{\mathrm{pot}}}{70}\right)^3(1+0.1V_{\mathrm{shear}})^{-2}, \quad \text{(A1)}$$

where η is absolute vorticity at 850 hPa (s^{-1}), H is relative humidity at 700 hPa (%), V_{pot} is potential intensity ($\mathrm{m\,s}^{-1}$) calculated using a routine provided by K. Emanuel (ftp://texmex.mit.edu/pub/emanuel/TCMAX/), and V_{shear} is vertical shear from 850 to 200 hPa ($\mathrm{m\,s}^{-1}$).

The Bruyère et al. (2012) index is defined as

$$\mathrm{CGI} = \left(\frac{V_{\mathrm{pot}}}{70}\right)^3(1+0.1V_{\mathrm{shear}})^{-2}. \quad \text{(A2)}$$

The Tippett et al. (2011) index is defined as

$$\mathrm{TIP} = \exp[b + b_\eta\eta + b_H H + b_T T + b_v V + \log(\cos\phi)], \quad \text{(A3)}$$

where η is clipped absolute vorticity at 850 hPa [$10^5\,\mathrm{s}^{-1}$; $\eta = \min(\eta, 3.7)$], $T = \mathrm{SST} - \overline{\mathrm{SST}}^{(20°\mathrm{S}-20°\mathrm{N})}$ (°C), ϕ is latitude, H is relative humidity at 600 hPa (%), and V is vertical shear from 850 to 200 hPa ($\mathrm{m\,s}^{-1}$). The constants used are those from line 6 of Tippett et al. (2011) (see Table 1) and as used by Menkes et al. (2012): $b = -5.8$, $b_n = 1.03$, $b_H = 0.05$, $b_T = 0.56$, and $b_V = -0.15$.

The Royer et al. (1998) index is defined as

$$\mathrm{YGP} = |f|\left(\zeta_r\frac{f}{|f|}+5\right)\left(\left|\frac{\delta V}{\delta P}\right|+3\right)^{-1}E\left(\frac{\delta\theta e}{\delta P}+5\right) \times \max\left[\min\left(\frac{\mathrm{RH}-40}{30},1\right),0\right],$$

where ζ_r is the relative vorticity at 925 hPa, the vertical wind shear $\delta V/\delta P$ is calculated between 925 and 200 hPa, the vertical gradient of equivalent potential temperature θ_e is calculated between the same levels, and RH is the average relative humidity between 700 and 500 hPa. A later version by Royer and Chauvin (2009) replaces the thermal terms in this equation (E and terms to the right of it) with a convective potential derived from the convective precipitation.

REFERENCES

Ballinger, A. P., T. M. Merlis, I. M. Held, and M. Zhao, 2015: The sensitivity of tropical cyclone activity to off-equatorial thermal forcing in aquaplanet simulations. *J. Atmos. Sci.*, **72**, 2286–2302, https://doi.org/10.1175/JAS-D-14-0284.1.

Best, M. J., and Coauthors, 2011: The Joint UK Land Environment Simulator (JULES), model description—Part 1: Energy and water fluxes. *Geosci. Model Dev.*, **4**, 677–699, https://doi.org/10.5194/gmd-4-677-2011.

Bister, M., and K. A. Emanuel, 1998: Dissipative heating and hurricane intensity. *Meteor. Atmos. Phys.*, **65**, 233–240, https://doi.org/10.1007/BF01030791.

Bruyère, C. L., G. J. Holland, and E. Towler, 2012: Investigating the use of a genesis potential index for tropical cyclones in the North Atlantic Basin. *J. Climate*, **25**, 8611–8626, https://doi.org/10.1175/JCLI-D-11-00619.1.

Camargo, S. J., 2013: Global and regional aspects of tropical cyclone activity in the CMIP5 models. *J. Climate*, **26**, 9880–9902, https://doi.org/10.1175/JCLI-D-12-00549.1.

——, M. K. Tippett, A. H. Sobel, G. A. Vecchi, and M. Zhao, 2014: Testing the performance of tropical cyclone genesis indices in future climates using the HiRAM model. *J. Climate*, **27**, 9171–9196, https://doi.org/10.1175/JCLI-D-13-00505.1.

Chavas, D. R., and K. Emanuel, 2014: Equilibrium tropical cyclone size in an idealized state of axisymmetric radiative–convective equilibrium. *J. Atmos. Sci.*, **71**, 1663–1680, https://doi.org/10.1175/JAS-D-13-0155.1.

——, K. A. Reed, and J. A. Knaff, 2017: Physical understanding of the tropical cyclone wind–pressure relationship. *Nat. Commun.*, **8**, 1360, https://doi.org/10.1038/s41467-017-01546-9.

Edwards, J. M., and A. Slingo, 1996: Studies with a flexible new radiation code. I: Choosing a configuration for a large-scale

model. *Quart. J. Roy. Meteor. Soc.*, **122**, 689–719, https://doi.org/10.1002/qj.49712253107.

Emanuel, K. A., 2010: Tropical cyclone activity downscaled from NOAA-CIRES reanalysis, 1908–1958. *J. Adv. Model. Earth Sys.*, **2**, 1, https://doi.org/10.3894/JAMES.2010.2.1.

——, 2013: Downscaling CMIP5 climate models shows increased tropical cyclone activity over the 21st century. *Proc. Natl. Acad. Sci. USA*, **110**, 12 219–12 224, https://doi.org/10.1073/pnas.1301293110.

——, and D. S. Nolan, 2004: Tropical cyclone activity and the global climate system. *26th Conf. on Hurricanes and Tropical Meteorology*, Miami, FL, Amer. Meteor. Soc., 10A.2, https://ams.confex.com/ams/26HURR/techprogram/paper_75463.htm.

——, and A. Sobel, 2013: Response of tropical sea surface temperature, precipitation, and tropical cyclone-related variables to changes in global and local forcing. *J. Adv. Model. Earth Syst.*, **5**, 447–458, https://doi.org/10.1002/jame.20032.

Fedorov, A. V., L. Muir, W. R. Boos, and J. Studholme, 2019: Tropical cyclogenesis in warm climates simulated by a cloud-system resolving model. *Climate Dyn.*, **52**, 107–127, https://doi.org/10.1007/s00382-018-4134-2.

Gray, W. M., 1968: Global view of the origin of tropical disturbances and storms. *Mon. Wea. Rev.*, **96**, 669–700, https://doi.org/10.1175/1520-0493(1968)096<0669:GVOTOO>2.0.CO;2.

——, 1975: Tropical cyclone genesis. Colorado State University Dept. of Atmospheric Science Paper 234, 121 pp.

Hayashi, Y.-Y., and A. Sumi, 1986: The 30–40 day oscillations simulated in an "aqua planet" model. *J. Meteor. Soc. Japan*, **64**, 451–467, https://doi.org/10.2151/jmsj1965.64.4_451.

Held, I. M., and M. Zhao, 2008: Horizontally homogeneous rotating radiative–convective equilibria at GCM resolution. *J. Atmos. Sci.*, **65**, 2003–2013, https://doi.org/10.1175/2007JAS2604.1.

Holland, G. J., 1983: Tropical cyclone motion: Environmental interaction plus a beta effect. *J. Atmos. Sci.*, **40**, 328–342, https://doi.org/10.1175/1520-0469(1983)040<0328:TCMEIP>2.0.CO;2.

Kalnay, E., and Coauthors, 1996: The NCEP/NCAR 40-Year Reanalysis Project. *Bull. Amer. Meteor. Soc.*, **77**, 437–471, https://doi.org/10.1175/1520-0477(1996)077<0437:TNYRP>2.0.CO;2.

Kanamitsu, M., W. Ebisuzaki, J. Woollen, S.-K. Yang, J. J. Hnilo, M. Fiorino, and G. L. Potter, 2002: NCEP–DOE AMIP-II Reanalysis (R-2). *Bull. Amer. Meteor. Soc.*, **83**, 1631–1643, https://doi.org/10.1175/BAMS-83-11-1631.

Kang, N.-Y., and J. B. Elsner, 2015: Trade-off between intensity and frequency of global tropical cyclones. *Nat. Climate Change*, **5**, 661–664, https://doi.org/10.1038/nclimate2646.

Khairoutdinov, M., and K. A. Emanuel, 2013: Rotating radiative-convective equilibrium simulated by a cloud-resolving model. *J. Adv. Model. Earth Syst.*, **5**, 816–825, https://doi.org/10.1002/2013MS000253.

Kim, H. M., P. J. Webster, and J. A. Curry, 2011: Modulation of North Pacific tropical cyclone activity by three phases of ENSO. *J. Climate*, **24**, 1839–1849, https://doi.org/10.1175/2010JCLI3939.1.

Knutson, T. R., and S. Manabe, 1995: Time-mean response over the tropical Pacific to increased CO_2 in a coupled ocean–atmosphere model. *J. Climate*, **8**, 2181–2199, https://doi.org/10.1175/1520-0442(1995)008<2181:TMROTT>2.0.CO;2.

Lock, A. P., A. R. Brown, M. R. Bush, G. M. Martin, and R. N. B. Smith, 2000: A new boundary layer mixing scheme. Part I: Scheme description and single-column model tests. *Mon. Wea. Rev.*, **128**, 3187–3199, https://doi.org/10.1175/1520-0493(2000)128<3187:ANBLMS>2.0.CO;2.

Ma, Z., J. Fei, L. Liu, X. Huang, and X. Cheng, 2013: Effects of the cold core eddy on tropical cyclone intensity and structure under idealized air–sea interaction conditions. *Mon. Wea. Rev.*, **141**, 1285–1303, https://doi.org/10.1175/MWR-D-12-00123.1.

——, ——, ——, and ——, 2017: An investigation of the influences of mesoscale ocean eddies on tropical cyclone intensities. *Mon. Wea. Rev.*, **145**, 1181–1201, https://doi.org/10.1175/MWR-D-16-0253.1.

Menkes, C. E., M. Lengaigne, P. Marchesiello, N. C. Jourdain, E. M. Vincent, J. Lefèvre, F. Chauvin, and J. F. Royer, 2012: Comparison of tropical cyclogenesis indices on seasonal to interannual timescales. *Climate Dyn.*, **38**, 301–321, https://doi.org/10.1007/s00382-011-1126-x.

Merlis, T. M., and I. M. Held, 2019: Aquaplanet simulations of tropical cyclones. *Curr. Climate Change Rep.*, **5**, 185–195, https://doi.org/10.1007/s40641-019-00133-y.

——, M. Zhao, and I. M. Held, 2013: The sensitivity of hurricane frequency to ITCZ changes and radiatively forced warming in aquaplanet simulations. *Geophys. Res. Lett.*, **40**, 4109–4114, https://doi.org/10.1002/grl.50680.

——, W. Zhou, I. M. Held, and M. Zhao, 2016: Surface temperature dependence of tropical cyclone-permitting simulations in a spherical model with uniform thermal forcing. *Geophys. Res. Lett.*, **43**, 2859–2865, https://doi.org/10.1002/2016GL067730.

Murakami, H., and B. Wang, 2010: Future change of North Atlantic tropical cyclone tracks: Projection by a 20-km-mesh global atmospheric model. *J. Climate*, **23**, 2699–2721, https://doi.org/10.1175/2010JCLI3338.1.

Rappin, E. D., and D. S. Nolan, 2012: The effect of vertical shear orientation on tropical cyclogenesis. *Quart. J. Roy. Meteor. Soc.*, **138**, 1035–1054, https://doi.org/10.1002/qj.977.

Reed, K. A., and D. R. Chavas, 2015: Uniformly rotating global radiative–convective equilibrium in the Community Atmosphere Model, version 5. *J. Adv. Model. Earth Syst.*, **7**, 1938–1955, https://doi.org/10.1002/2015MS000519.

Royer, J. F., and F. Chauvin, 2009: Response of tropical cyclogenesis to global warming in an IPCC AR4 scenario. *Hurricanes and Climate Change*, J. Elsner and T. Jagger, Eds., Springer, 213–234.

——, ——, B. Timbal, P. Araspin, and D. Grimal, 1998: A GCM study of the impact of greenhouse gas increase on the frequency of occurrence of tropical cyclones. *Climatic Change*, **38**, 307–343, https://doi.org/10.1023/A:1005386312622.

Schade, L. R., and K. A. Emanuel, 1999: The ocean's effect on the intensity of tropical cyclones: Results from a simple coupled atmosphere–ocean model. *J. Atmos. Sci.*, **56**, 642–651, https://doi.org/10.1175/1520-0469(1999)056<0642:TOSEOT>2.0.CO;2.

Sharmila, S., and K. J. E. Walsh, 2017: Impact of large-scale dynamic versus thermodynamic climate conditions on contrasting tropical cyclone genesis frequency. *J. Climate*, **30**, 8865–8883, https://doi.org/10.1175/JCLI-D-16-0900.1.

——, ——, M. Thatcher, S. Wales and S. Utembe, 2020: Real world and tropical cyclone world. Part I: High-resolution climate model verification. *J. Climate*, **33**, 1455–1472, https://doi.org/10.1175/JCLI-D-19-0078.1.

Shi, X., and C. S. Bretherton, 2014: Large-scale character of an atmosphere in rotating radiative-convective equilibrium. *J. Adv. Model. Earth Syst.*, **6**, 616–629, https://doi.org/10.1002/2014MS000342.

Sugi, M., A. Noda, and N. Sato, 2002: Influence of the global warming on tropical cyclone climatology: An experiment with the JMA global model. *J. Meteor. Soc. Japan*, **80**, 249–272, https://doi.org/10.2151/jmsj.80.249.

Tippett, M. K., S. J. Camargo, and A. H. Sobel, 2011: A Poisson regression index for tropical cyclone genesis and the role of

large-scale vorticity in genesis. *J. Climate*, **24**, 2335–2357, https://doi.org/10.1175/2010JCLI3811.1.

Vecchi, G. A., and B. J. Soden, 2007: Global warming and the weakening of the tropical circulation. *J. Climate*, **20**, 4316–4340, https://doi.org/10.1175/JCLI4258.1.

Viale, F., and T. M. Merlis, 2017: Variations in tropical cyclone frequency response to solar and CO_2 forcing in aquaplanet simulations. *J. Adv. Model. Earth Syst.*, **9**, 4–18, https://doi.org/10.1002/2016MS000785.

Walters, D. N., and Coauthors, 2017: The Met Office Unified Model Global Atmosphere 6.0/6.1 and JULES Global Land 6.0/6.1 configurations. *Geosci. Model Dev.*, **10**, 1487–1520, https://doi.org/10.5194/gmd-10-1487-2017.

Wilson, D. R., A. C. Bushell, A. M. Kerr-Munslow, J. D. Price, and C. J. Morcrette, 2008: PC2: A 1176 prognostic cloud fraction and condensation scheme. I: Scheme description. *Quart. J. Roy. Meteor. Soc.*, **134**, 2093–2107, https://doi.org/10.1002/qj.333.

Wing, A. A., S. J. Camargo, and A. H. Sobel, 2016: Role of radiative–convective feedbacks in spontaneous tropical cyclogenesis in idealized numerical simulations. *J. Atmos. Sci.*, **73**, 2633–2642, https://doi.org/10.1175/JAS-D-15-0380.1.

Zhou, W., 2015: The impact of vertical shear on the sensitivity of tropical cyclogenesis to environmental rotation and thermodynamic state. *J. Adv. Model. Earth Syst.*, **7**, 1872–1884, https://doi.org/10.1002/2015MS000543.

——, I. M. Held, and S. T. Garner, 2014: Parameter study of tropical cyclones in rotating radiative–convective equilibrium with column physics and resolution of a 25-km GCM. *J. Atmos. Sci.*, **71**, 1058–1069, https://doi.org/10.1175/JAS-D-13-0190.1.

——, ——, and ——, 2017: Tropical cyclones in rotating radiative–convective equilibrium with coupled SST. *J. Atmos. Sci.*, **74**, 879–892, https://doi.org/10.1175/JAS-D-16-0195.1.